Geomechanics and Engineering, *Vol. 18, No. 3 (2019) 329-337*
DOI: https://doi.org/10.12989/gae.2019.18.3.329

Visualization of bulging development of geosynthetic-encased stone column

Yang Zhou[1a], Gangqiang Kong[*1], Huaifeng Peng[1a], Chunhong Li[1a] and Hongyu Qin[2b]

[1]Key Laboratory of Geomechanics and Embankment Engineering in Ministry of Education, Hohai University, No.1 Xikang Road, Nanjing, China
[2]Flinders University,1284 Clovelly Park South Australia 5042, Australia

(Received April 20, 2018, Revised May 22, 2019, Accepted June 4, 2019)

Abstract. This paper presents an experimental investigation about visualization of bulging development of geosynthetic-encased stone column (GESC) based on the digital image correlation (DIC) technique and transparent soil. Visual model tests on GESC and ordinary stone column (OSC) were carried out. In order to delete the warping effect resulting from transparent soil and experiment setup, a modification for experiment results was performed. The bulging development process of the GESC and the displacement field of the surrounding soil were measured. By comparing with the existing experimental and theoretical results, it demonstrates that the model test system developed for studying the continuous bulging development of GESC is suitable. The current test results show that the bulging depth of GESC ranges from 1.05 to 1.40 times the diameter of GESC. The influence depth of GESC bulging on surrounding soil displacement is 0~3 the times diameter of GESC.

Keywords: geosynthetic-encased stone column; transparent soil; visualization; bulging development; displacement field

1. Introduction

Geosynthetic-encased stone column (GESC) is a ground improvement technique for soft soils, which reduces the total settlements and accelerates consolidation. Compared with ordinary stone column (OSC), GESC has greater bearing capacity and undergoes less radial bulging. The behavior of GESC has been investigated through in-situ field tests (Yoo 2010, Almeida and Riccio 2015) and model tests (Lee *et al.* 2007, Sivakumar *et al.* 2007, Malarvizhi and Ilamparuthi 2007, Gniel and Bouazza 2009, Murugesan and Rajagopal 2010, Shivashankar *et al.* 2010, Ali *et al.* 2012, Afshar and Ghazavi 2014, Hong *et al.* 2016, Demir and Sarici 2017). Particularly, sand ground was selected as surrounding soil in model tests performed by Lee *et al.* (2007). In these studies, the bulging of OSC and GESC was visualized by carefully removing the stones and casting plaster (Murugesan and Rajagopal 2010) or pouring concentrated slurry to shape (Shivashankar *et al.* 2010). The operation is complex and only the last bulging state is visible. The study of bulging development is helpful for understanding the bearing mechanism of stone columns. Nevertheless, the internal displacement field, soil movements and radial bulging development during loading are difficult to measure accurately. This can be solved by using innovative techniques such as transparent soil and digital image correlation (DIC).

Transparent soil, made from fused quartz and pore fluid with the same refractive index, has been used to model soil (Ezzein and Bathurst 2014, Guzman *et al.* 2014). The visual model technique in combination with the DIC technique and transparent soil have been used in model tests to study internal deformation problems (Chen *et al.* 2014, Ezzein and Bathurst 2014, Kong *et al.* 2015). These studies confirm that the transparent soil technique is an effective method for visualizing the displacement field. Particularly, MacKelvey (2002, 2004) used a transparent soil to allow visual monitoring of OSCs under vertical load. However, the primary purpose of their study was the failure pattern of short and long OSCs. The exact bulging, bulging development process and displacement field of surrounding soil were not measured. The soil was in a passive state when the bulging happens. Model tests using transparent soil like grout permeation (Liu *et al.* 2013), plie-deformation induced ground movement (Liu *et al.* 2010; Hird *et al.* 2011) proved the feasibility of simulating natural soil by transparent soil in passive state.

In this study, model tests were carried out to investigate the characteristics of GESC using transparent soil and DIC technique. The radial bulging development with increasing load was obtained. The displacement field of the surrounding soil was also measured. Furthermore, the deformation results in these tests were compared with those obtained from previous model tests and predicted by existing theory.

2. Experimental description

2.1 Model test setup

The visual model test setup, shown in Fig. 1(a),

*Corresponding author, Professor
E-mail: gqkong1@163.com
[a]Ph.D. Student
[b]Ph.D.

http://www.techno-press.org/?journal=gae&subpage=7
ISSN: 2005-307X (Print), 2092-6219 (Online)

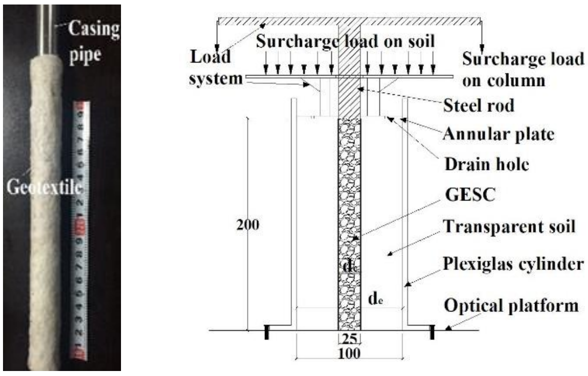

(a) Test setup (b) Elevation view

Fig. 1 Schematic diagram of apparatus

Table 1 Chracteristic values used for model to prototype scaling

Dimensionless factor	Characteristic	Scaling factor (prototype/model)	Prototype value	Model value
$\pi_1=J/\rho gH^2$	J (kN/m)	λ^2 (=400)	200 ~ 4000	0.5 ~ 10
$\pi_2=T/\rho gH^2$	T (kN/m)	λ^2 (=400)	40 ~ 4000	0.1 ~ 10
$\pi_3=D/H$	D (m)	λ (=20)	0.2 ~ 1	0.01 ~ 0.05

consisted of a linear laser, a charge-coupled device (CCD) camera, a load system, an optical platform, transparent soil, GESC (or OSC), a plexiglas cylindrical model box and a computer for image processing. The linear laser (EP 532-2W) can produce a vertical or lateral light sheet. The CCD camera with a resolution of 1280 × 960 was approximately positioned 500 mm away from the laser sheet. A schematic of the load test in a unit cell and loading arrangement is showed in Fig. 1(b).

The unit-cell idealization is used in this study to simplify the design of the apparatus. Ambily and Gandhi (2007), Gniel and Bouazza (2009), Murugesan and Rajapopal (2010), Nayak *et al.* (2011) have used this concept of a unit cell in their model tests to assess the behavior of a stone column at the centre of a large group. In order to achieve the unit cell model, a plexiglas cylinder, 10 mm thickness, 100 mm inner diameter (d_e) and 230 mm height, was used in the model test. The diameter of the OSC and GESC (d_c) was 25 mm. The dimension of the adopted unit cell is equivalent to stone column installed at a centre-to-centre spacing of 88 mm ($3.5d_c$) in a square pattern or 95 mm ($3.8d_c$) in a triangular pattern. The loading system includes two parts which can apply loads to the column and soil respectively, as shown in Fig. 1(b). One part is a steel rod of "T" shape with the same diameter as the stone column. It can apply pressure on the GESC or OSC through dead weights placed symmetrically on the hanger. The other part includes a hollow steel pipe with a rectangular steel plate welded on the top and an annular plate welded at the bottom. It can apply pressure to the transparent soil surrounding the column by dead weight on the top plate. Holes were perforated on the annular plate to allow drainage. The casing pipe has an outer diameter of 25 mm with thickness of 0.2 mm. The height of the GESC or OSC is 200 mm.

Table 1 shows the scaling factors for the model and

Table 2 Mechanical properties of the model test materials

Materials	Parameter	unit	value
Transparent soil	Coefficient of uniformity		3.38
	Coefficient of curvature		1.19
	Maximum dry unit weight	kN/m^3	13.00
	Minimum dry unit weight	kN/m^3	9.9
	Saturated unit weight (γ_s)	kN/m^3	18.37
	Peak friction angle (φ_s)*	°	37
	Cohesion (c)	kPa	0
	One-dimensional constraint ymodulus (E_s)	MPa	8.12
	Compression index (C_c)		0.04
Stone column	Coefficient of uniformity		2.62
	Coefficient of curvature		0.96
	Peak friction angle (φ_c)	°	41
	Saturated unit weight (γ_c)	kN/ m^3	19.10
Geotextile	Thickness	mm	1
	Tensile strength with seam (T)	kN/m	0.51
	Strain at peak strength with seam	%	62.09
	Tensile modulus with seam (J)	kN/m	0.82

*from consolidation-drained test after Kong *et al.* (2015)

prototype with the same stone aggregates density. The model GESC of 0.025 m in diameter was chosen to simulate a prototype column of 0.5 m in diameter, the ratio of prototype column diameter to the model column diameter (λ) is 20. Therefore, stresses on a full-scale GESC are 20 times those measured on model GESC.

2.2 Properties of materials

Transparent soil, crushed stone aggregate and geotextile were used in this investigation. The transparent soil was manufactured by fused quartz and oil-based solution with the same refractive index of 1.4585. The transparent soil had a uniform gradation and the particle size distribution is shown in Fig. 2(a), along with those used in previous researches for comparison. As followed the previous studies of stone column or geosynthetic-stone column surrounding by natural soil, the particle size of stone column material was similar to that in these model tests (Ambily and Gandhi (2007), Gniel and Bouazza (2009), Murugesan and Rajapopal (2010), Nayak *et al.* (2011)) when the transparent soil was similar to natural soil. The properties of the fused quartz are presented in Table 2. The oil-based solution, made of mixed mineral oil and Norpar 12 fluid (4:1 ratio by weight), has a refractive index of 1.4585 at 24°C (Zhao *et al.* 2010). More details obtained by consolidated-drained triaxial tests about the transparent soil can be found in Kong *et al.* (2015). The cohesion was calculated as 0. Hence, the transparent soil was model as a typical sand.

The stone aggregates used to form the stone column were angular granite chips of size 1-10 mm and had uniform gradation. The gradation curve of the stone aggregates is shown in Fig. 2(a). By controlling the volume of the stone chips and the weight filling in the casing pipe, a

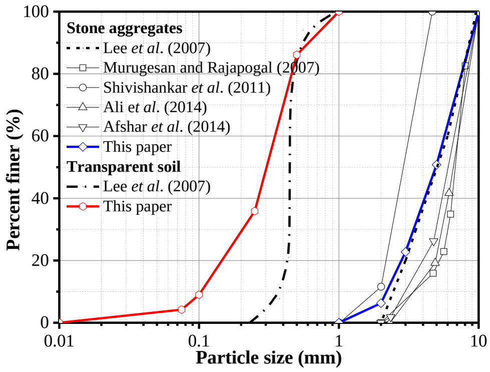

(a) Particle size distributions

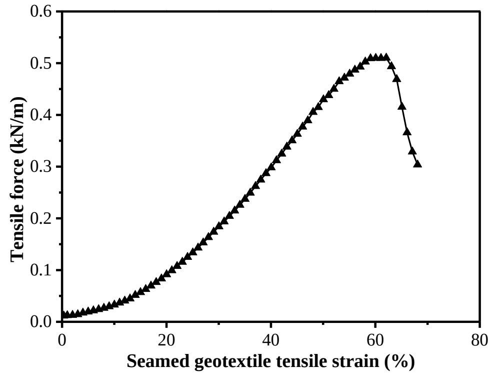

(b) Tensile-strain curves of geotextile

Fig. 2 The properities of the model test materials

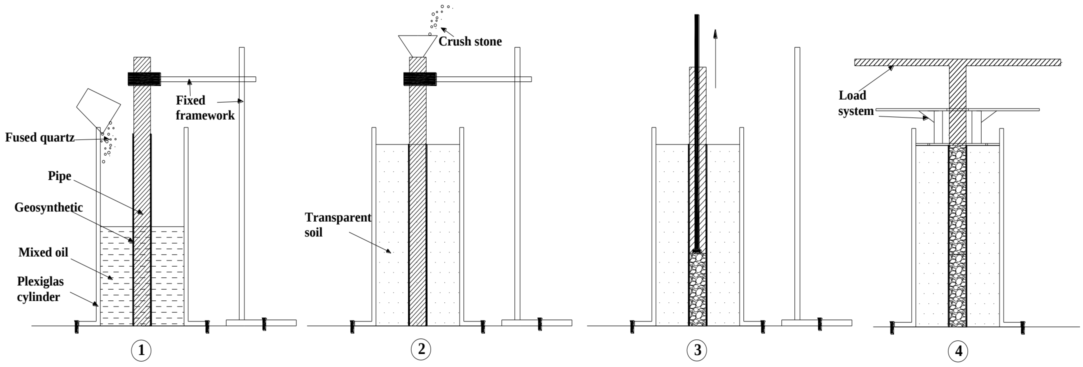

Fig. 3 GESC installation process

column was made with a relative density of approximately 70%. The properties of the stone aggregate were also presented in Table 2. Casing geotextile was made of nonwoven geotextile. The tensile force-strain relationship of the tested geotextile samples under standard wide-width tension tests (ASTM D4595) was shown in Fig. 2(b). Since the encasement was formed by stitching a piece of geotextile into a sleeve, the tensile-strain relationship of the seamed sample of the geotextiles were tested. The tensile strength properties of the geotextiles are listed in Table 2.

2.3 Installation of GESC/OSC

The installation process was schematically shown in Fig. 3. It mainly includes the following steps:

• Preparing casing pipe: The casing pipe was used to install the stone column. It was wrapped with geotextile and fixed at the centre of the plexiglas cylinder, through a fixed framework.

• Placing soil and column: First, fused quartz was poured into pore fluid of mixed oil by the sand raining method (Madabhushi *et al.* 2006) (400 mm high from the surface). Second, a panel with small holes was placed on the soil sample. The soil sample had a relative density of about 60% after pressure on the panel. Then stone aggregates were poured into the casing pipe in 5 layers.

• Constructing of GESC: After placing each layer of the stone aggregate, the stone aggregate was compacted with a tamping rod (10 mm in diameter and 500 mm long). This process was repeated four times until the entire height of the stone column was formed.Then the casing pipe was lifted up gently and the geosynthetic stayed with the stone column. Extra pore fluid was drained out and extracted by a suction bulb.

• Setting up the loading and measuring system: Upon completing the stone column installation, the loading system was placed on the top of the soil and column. The measuring system was set around the plexiglas cylinder, with linear laser and CCD camera across.

2.4 Loading test on GESC/OSC

As described earlier, the loading system can apply different loads to the column and soil, respectively. Since the GESCs are usually used in column-supported embankment, deformation of column is not same as the one of soil (Alamgir *et al.* 1996). Hence, the rigid plate loading method seems not proper. The pressure on the GESC was set as the known value based on a given stress concentration ratio in these tests. The pressure applied to the column and soil was determined by

$$q_c = nq_s = \frac{n}{1+\alpha(n-1)}q \tag{1}$$

where q is the total applied pressure with a range of 0~50 kPa in this paper; q_c and q_s are the pressure applied to the column and soil, respectively; n $(=q_c/q_s)$ is the stress

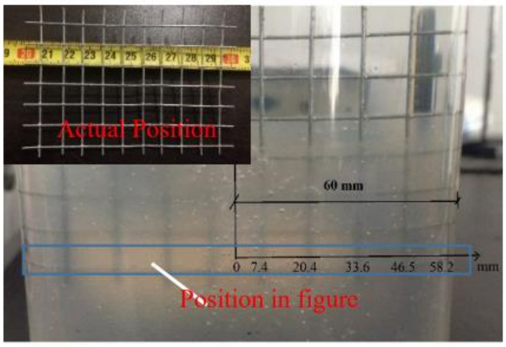

(a) Diagram of modification method

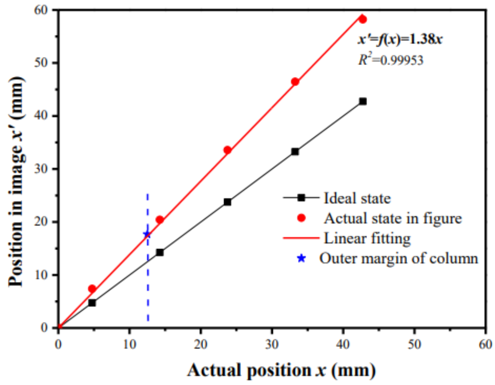

(b) Results of modification method

Fig. 4 Modification for horizontal position between actual and image

concentration factor. Castro and Sagaseta (2011) concluded from their study that the value of n ranges from 5 to 10.

In this study, the stress concentration factor (n) was assumed as 5, as proposed by Zhang and Zhao (2015).

α is the area replacement ratio, defined as follows

$$\alpha = \frac{A_c}{A_e} = \frac{d_c^2}{d_e^2} \tag{2}$$

where A_e and A_c are the entire area of the cylindrical unit cell and cross-sectional area of the column, respectively; d_e and d_c are the diameter of unit cell and diameter of stone column, respectively.

2.5 Digital image correlation (DIC) technique

As the interaction between laser light and transparent soil produces a distinctive speckle pattern. Small particle movement can result in the speckle distribution changing in the plane of measurement. Images captured before and after deformation were analyzed by the DIC technique. The images were split into a large number of interrogation windows. For each of these interrogation window, a DIC displacement vector was produced before and after each increment of load pressure with the help of an autocorrecting technique. Performing this for all interrogation regions produces a vector map of the average particle displacements. The discrete form of the standard cross-correlation function is as follows

$$C(\Delta x, \Delta y) = \frac{1}{MN} \sum_{m=0}^{M-1} \sum_{n=0}^{N-1} f(m,n) g(m+\Delta x, n+\Delta y) \tag{3}$$

where M and N are the dimensions of interrogated images, and f and g are the grayscale intensities of the two images being interrogated. The spatial displacement field can be obtained from the displacement in each interrogated window.

2.6 Warping effect and modification

According Snell's law from curved surfaces, warping effect will make difference between position in DIC images and in actual. Plexiglas cylinder is like a magnifying glass when the objects in the cylinder are photographed. In order to eliminate this effect, it is necessary to modify the displacement results obtained from DIC technique. The displacements were calculated by cross-correlating images from same cross section on the physical coordinate plane. The distance between two outside marines of cylinder is 120 mm (diameter and thickness of cylinder). The surface is linear along vertical direction because of the cylinder surface, rather than spherical surface. On account of cylinder is only radial-curved, the warping effect along vertical orientation is ignored. A simple test was using to measure the effect in this study.

As shown in Fig. 4(a), metal-grid with width of 100 mm was inserted into transparent soil in cylinder. The width of every grid is 9.5 mm. The center of the metal-grid is set as the starting point of the physical coordinate at horizontal orientation. The position of each grid joint were measured by photo and compared with metal-grid in actual. The details of linear difference are shown in Fig. 4(b).

3. Test results and discussions

3.1 Deformation of GESC/OSC

The detailed test parameters were list in Table 3. The pressure-deformation responses observed for OSC and GESC are shown in Figs. 5 and 6, respectively. Fig. 5 shows the physical photos and the bulging distribution at a total applied pressure of 50 kPa. The bulging distribution of GESC or OSC obtained by DIC technique and then modified were plotted in this figure. Fig. 6 plotted the deformation of GESC or OSC (settlement and bulging). The radial bulges of GESC or OSC before and after modification are δ'_c and δ_c respectively. Fig. 6(a) plots the applied pressure (q) against the normalized settlement (S_c/d_c). The test results obtained by Murugesan and Rajagopal (2010) using clay soil and by Ali *et al.* (2012) using Kaolinite clay are also presented for comparison. In the figure, the general variation pattern of q-S_c/d_c relationship was similar. Furthermore, at q = 50 kPa, the settlement of GESC (S_c/d_c = 0.244) is about 50% of that of the OSC (S_c/d_c = 0.479). This demonstrates the use of transparent soil is feasible in GESC model tests. The bulking of columns was usually taken into consideration for

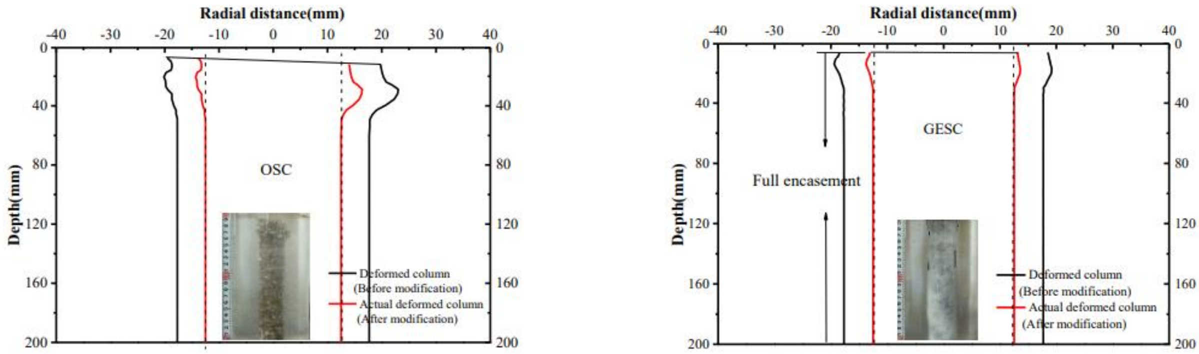

(a) OSC (b) GESC

Fig. 5 Deformed column under pressure of 50 kPa

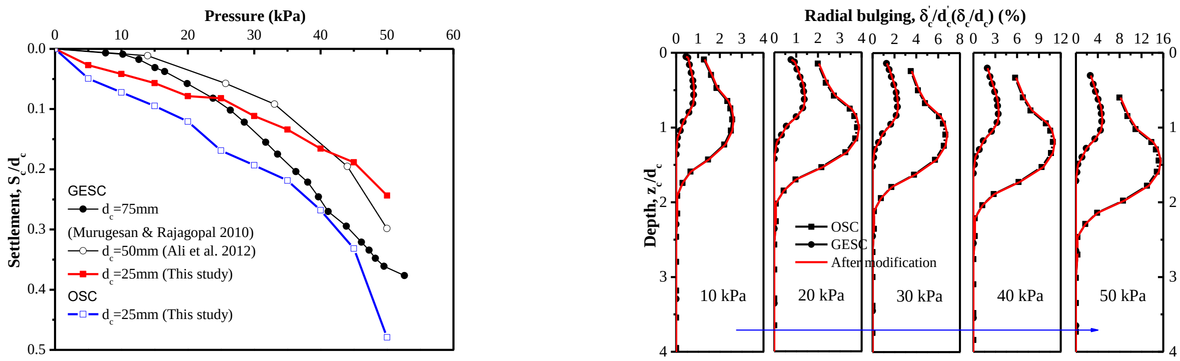

(a) Pressure – settlement curves (b) Radial bulging with depth

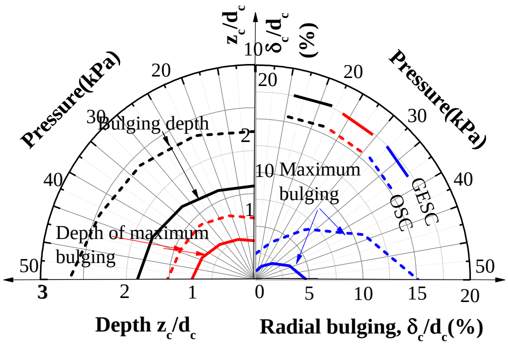

(c) Bulging development

Fig. 6 Deformation development of column

Table 3 Detailed test parameters

Test description	Diameters of columns (mm)	Lengths of columns (mm)	Applied load (kPa)	Encasement length (mm)
OSC	25	200	0	0
OSC	25	200	10	0
OSC	25	200	20	0
OSC	25	200	30	0
OSC	25	200	40	0
OSC	25	200	50	0
GESC	25	200	0	200
GESC	25	200	10	200
GESC	25	200	20	200
GESC	25	200	30	200
GESC	25	200	40	200
GESC	25	200	50	200

the super-long column. In the study, the ratio that length to diameters (200/25=8) is not so large. Hence, the possibility of buckling was ignored in the study.

Fig. 5(b) shows the pressure settlement curves of the surrounding soil. Compared with OSC, GESC reduces the soil deformation nearly by 30% (S/d_c = 0.198 and 0.279 for GESC and OSC encased under 50 kPa, respectively). It clearly shows that the stone column with geosynthetic encasement has undergone minor vertical settlement (S_c) and radial bulging deformation (δ_c) at the top of the column. Fig. 6(b) presents the normalized radial bulging (δ_c/d_c) development process observed along the normalized length of the column (z_c/d_c) with and without geosynthetic encasement under 10, 20, 30, 40 and 50 kPa. It can be seen that the deformation shape of the GESC is similar to that of the OSC, but the maximum bulging, the depth of maximum bulging and bulging depth varies. Bulging depth (z_b), the maximum radial bulging and the depth of the maximum

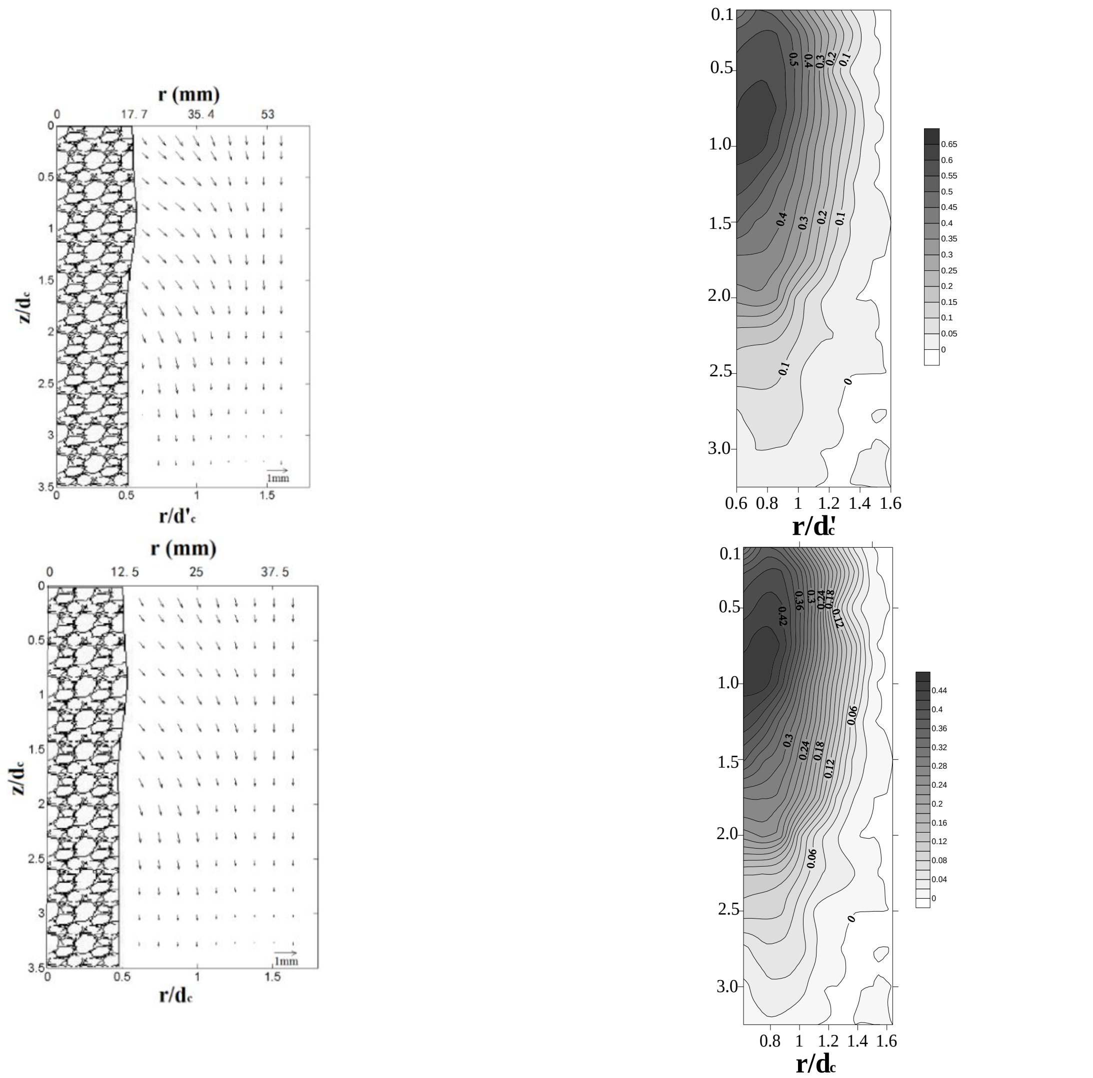

(a) Vectors before and after modification (b) Radial contours before and after modification

Fig. 7 Normalized displacement field of surrounding soil under pressure of 40 kPa

bulging were three important measurements characterizing radial bulging. Fig. 6(c) plots development of these characteristic measurements, specifically. The maximum radial bulging of GESC of 0.83%, 1.41%, 2.33%, 3.49% and 4.86% occurs at depth z_c/d_c of 0.45~0.75. By contrast, the maximum bulging (δ_c/d_c) of OSC of 2.63%, 3.88%, 6.83%, 11.19%, and 15.54% occurs at depth z_c/d_c of 0.7~1.2. The maximum radial bulging of GESC reduces by 70% compared with that of OSC. The bulging depth of GESC (z_c/d_c) ranges from 1.05~1.4 and 1.72~2.16 for GESC and OSC, respectively. This is consistent with the findings of Lee *et al.* (2007), who performed model tests and observed that bulging occurs at a depth 1~2.5 times the diameter of OSC.

3.2 Displacement of surrounding soil

The displacement of soil was measured before and after each increment of pressure by DIC technique and then modified by modification coefficient, as describe before. Under various pressures, the pattern of vector and contours (contains radial direction and vertical direction) are similar to each other. The vector and contours before and after modification at 40 kPa are plotted for demonstration, as shown in Fig. 7.

The horizontal and vertical axis represents the normalized radial distance (before modification r/d'_c and after modification r/d_c) and normalized depth z_c/d_c, respectively. It's clear that the maximum displacement of the soil occurs at about the depth of maximum bulging of GESC. The displacement field of the surrounding soil agrees well with the radial bulging shape of GESC.

Furthermore, the horizontal displacement attenuates along radial distance. The horizontal displacement of soil ranges from 0~1.57 d_c. When the normalized depth z_c/d_c reaches 3, the horizontal displacement is nearly not appreciable. This demonstrates the influence depth of GESC bulging on surrounding soil is 0~3 times diameter of GESC.

3.3 Comparison validation

In order to compare the bulging deformation of GESC using transparent soil with that using ordinary clay, the test

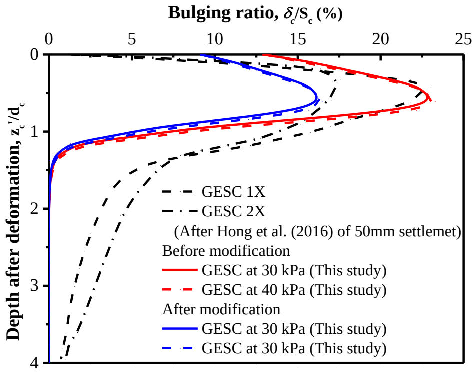

Fig. 8 Variation of bulging ratio with depth

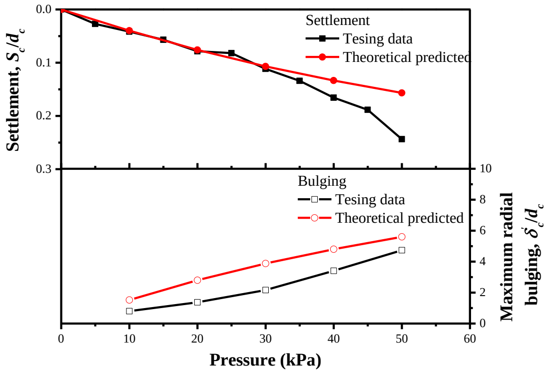

Fig. 9 Comparison of deformation with pressure

results are further analyzed. A bulging ratio is introduced and defined as δ_c/S_c. Fig. 8 shows the variation of bulging ratio with depth (after deformation z'_c/d_c).

The results of ET1X (J=0.34 kN/m) and ET2X (J=0.48 kN/m) in Hong *et al.* (2016) are also analyzed and presented.

The applied pressure is 30~40 kPa when the deformation of the stone column was measured in Hong *et al.* (2016). Hence bulging ratios at pressures of 30 and 40 kPa were chosen for comparison. The bulging shapes are closely matched in this figure. The maximum bulging ratios in this study are about 24% and are close to the 23% (ET2X) and the 17.5% (ET1X). The depth of maximum bulging is 0.4 and 0.35 times the diameter of the GESC in Hong *et al.* (2016), consistent with the results in the current study. The comparison demonstrates the validity of bulging deformation shape for GESC in transparent soil. It is worth noting that the bulging depth is quite different from that of Hong *et al.* (2016), which may be due to the higher friction angle of transparent soil compared to clay.

The measured deformation behavior of the single GESC at any depth was also predicted using a simple analytical model based on the unit-cell theory proposed by Kong *et al.* (2018). In their theoretical model, it was assumed that the geotextile material behaves as a nonlinear elastic material. The approximate calculation model were shown in Appendix. The detailed description could be refereed to Kong *et al.* (2018). Settlement (S_c/d_c) and maximum radial bulging (δ'_c/d_c) are meaningful focus in engineering cases. In order to quantify the deformation, the comparison analysis were conduct. Fig. 9 plots the deformation against the total applied pressure.

A reasonably good agreement is obtained between the theoretic calculation and model test results for settlement under relative low pressure. The results of maximum radial bulging (δ'_c/d_c) are slightly smaller than that obtained by theoretical predicted. That might be caused by the assumption that stone material is a nonlinear material.

4. Conclusions

The bulging development of a GESC was measured by conducting model tests using transparent soil and DIC technique. With an innovative experimental apparatus developed, major conclusions could be drawn as follows:

• The continuous bulging development of GESC (including bulging depth, the maximum bulging and the depth of maximum bulging) and the displacement field of surrounding soil can be obtained by using transparent soil and DIC techniques.

• Compared with OSC, the settlement and bulging of GESC reduce by 50% to 70%. The bulging depth and the depth of maximum bulging of GESC ranges from 1.05~1.40 and 0.45~0.75 times the diameter of GESC.

• The displacement field of the surrounding soil agrees well with the radial bulging shape of GESC. The radial displacement of soil ranges from 0~1.57 times the diameter of GESC. The influence depth of GESC bulging on surrounding soil is 0~3 the times diameter of GESC.

Acknowledgments

The research was financially supported by the National Science Foundation of China (Nos. 51639002, 51778212).

References

Afshar, J.N. and Ghazavi, M. (2014), "Experimental studies on bearing capacity of geosynthetic reinforced stone columns", *Arab. J. Sci. Eng.*, **39**(3), 1559-1571. https://doi.org/10.1007/s13369-013-0709-8.

Alamgir, M., Miura, N., Poorooshasb, H.B. and Madhav, M.R. (1996), "Deformation analysis of soft ground reinforced by columnar inclusions", *Comput. Geotech.*, **18**(4), 267-290. https://doi.org/10.1016/0266-352X(95)00034-8.

Ali, K., Shahu, J.T. and Sharma, K.G. (2012), "Model tests on geosynthetic-reinforced stone columns: A comparative study", *Geosynth. Int.*, **19**(4), 292-305. http://dx.doi.org/10.1680/gein.12.00016.

Ambily, A.P. and Gandhi, S.R. (2007), "Behavior of stone columns based on experimental and FEM analysis", *J. Geotech. Geoenviron. Eng.*, **133**(4), 405-415. https://doi.org/10.1061/(ASCE)1090-0241(2007)133:4(405).

ASTM D4595 (1986), *Standard Test Method for Tensile Properties of Geotextiles by Wide-Width Strip Method*, in *Annual Book of ASTM Standards*, ASTM International, West Conshohocken, Pennsylvania, U.S.A.

Black, J.A., Sivakumar, V., Madhav, M.R. and Hamill, G.A. (2007), "Reinforced stone columns in weak deposits: Laboratory model study", *J. Geotech. Geoenviron. Eng.*, **133**(9), 1154-1161. https://doi.org/10.1061/(ASCE)1090-0241(2007)133:9(1154).

Castro, J. and Sagaseta, C. (2011), "Deformation and consolidation around encased stone columns", *Geotext. Geomembranes*, **29**(3), 268-276. https://doi.org/10.1016/j.geotexmem.2010.12.001.

Chen, Z., Omidvar, M., Iskander, M. and Bless, S. (2014), "Modelling of projectile penetration using transparent soils", *Int. J. Phys. Modell. Geotech.*, **14**(3), 68-79. https://doi.org/10.1680/ijpmg.14.00003.

Demir, A. and Sarici, T. (2017), "Bearing capacity of footing supported by geogrid encased stone columns on soft soil", *Geomech. Eng.*, **12**(3), 417-439. https://doi.org/10.12989/gae.2017.12.3.417.

Ezzein, F.M. and Bathurst, R.J. (2014), "A new approach to evaluate soil-geosynthetic interaction using a novel pullout test apparatus and transparent granular soil", *Geotext. Geomembranes*, **42**(3), 246-255. https://doi.org/10.1016/j.geotexmem.2014.04.003.

Guzman, I.L., Iskander, M., Suescun-Florez, E. and Omidvar, M. (2014), "A transparent aqueous-saturated sand surrogate for use in physical modeling", *Acta. Geotech.*, **9**(2), 187-206. https://doi.org/10.1007/s11440-013-0247-2.

Gniel, J. and Bouazza, A. (2009), "Improvement of soft soils using geogrid encased stone columns", *Geotext. Geomembranes*, **27**(3), 167-175. https://doi.org/10.1016/j.geotexmem.2008.11.001.

Hird, C.C., Ni, Q. and Guymer, I. (2011), "Physical modeling of deformations around piling augers in clay", *Géotechnique*, **61**(11), 993-999. https://doi.org/10.1680/geot.9.T.028.

Hosseinpour, I., Almeida, M.S.S. and Riccio M (2015), "Full-scale load test and finite-element analysis of soft ground improved by geosynthetic-encased granular columns", *Geosynth. Int.*, **22**(6), 428-438. https://doi.org/10.1680/gein.15.00023.

Hong, Y.S., Wu, C.S. and Yu, Y.S. (2016), "Model tests on geotextile-encased granular columns under 1-g and undrained conditions", *Geotext. Geomembranes*, **44**(1), 13-17. https://doi.org/10.1016/j.geotexmem.2015.06.006.

Kong, G.Q., Liu, L., Liu, H.L. and Zhou, H. (2013), "Triaxial tests on deformation characteristics of transparent glass sand", *Chin. J. Geotech.*, **35**(6), 1140-1146 (in Chinese).

Kong, G.Q., Cao, Z.H., Zhou, H. and Sun, X.J. (2015), "Analysis of piles under oblique pullout load using transparent-soil models", *Geotech. Test. J.*, **38**(5), 725-738. https://doi.org/10.1520/GTJ20140109.

Kong, G.Q., Zhou, Y. and Liu, H.L. (2018), "Nonlinear model analysis of radial bulging deformation of geosynthetic-encased stone columns", *Int. J. Geomech.*, **18**(10), 06018022. https://doi.org/10.1061/(ASCE)GM.1943-5622.0001195.

Lee, D., Yoo, C. and Park, S. (2007), "Model tests for analysis of load carrying capacity of geogrid encased stone column", *Proceedings of the 17th International Offshore and Polar Engineering Conference*, Cupertino, Califrornia, U.S.A., July.

Liu, J.Y., Liu, M.L. and Gao, H.M. (2010), "Influence of pile geometry on internal sand displacement around a laterally loaded pile using transparent soil", *Proceedings of the Geoshanghai 2010*, Shanghai, China, June.

Liu, J., Gao, Y. and Sui, W. (2013), "Visualization of grout permeation inside transparent soil", *Proceedings of the 2nd International Conference on Geotechnical and Earthquake Engineering*, Chengdu, China, October.

Malarvizhi, S.N. and Ilamparuthi, K. (2007), "Comparative study on the behavior of encased stone column and conventional stone column", *Soils. Found.*, **47**(5), 873-885. https://doi.org/10.3208/sandf.47.873.

MacKelvey, D. (2002), "Performance of virbo stone column reinforced foundations in deep soft clay", Ph.D. Thesis, Queen's University, Belfast, U.K.

MacKelvey, D., Sivakumar, V., Bell, A. and Graham, J. (2004), "Modelling vibrated stone columns in soft clay", *Proc. Inst. Civ. Eng. Geotech. Eng.*, **157**(3), 137-149. https://doi.org/10.1680/geng.2004.157.3.137.

Madabhushi, S.P.G., Houghton, N.E. and Haigh, S.K. (2006), "A new automatic sand pourer for model preparation at University of Cambridge", *Proceedings of the 6th International Conference on Physical Modelling in Geotechnics*, Hong Kong, China, August.

Murugesan, S. and Rajagopal, K. (2010), "Studies on the behavior of single and group of geosynthetic-encased stone columns", *J. Geotech. Geoenviron. Eng.*, **136**(1), 129-139. https://doi.org/10.1061/(ASCE)GT.1943-5606.0000187.

Nayak, S., Shivashankar, R. and Ramanaidu, M. (2011), "Performance of stone columns with circumferential nails", *Proc. Inst. Civ. Eng. Ground Improv.*, **164**(12), 97-106. https://doi.org/10.1680/grim.2011.164.2.97.

Shivashankar, R., Badu, M.R.D., Nayak, S. and Manjunath, R. (2010), "Stone columns with vertical circumferential nails-laboratory model study", *Geotech. Geol. Eng.*, **28**(4), 695-706. https://doi.org/10.1007/s10706-010-9329-1.

Yoo, C. (2010), "Performance of geosynthetic-encased stone columns in embankment construction: Numerical investigation", *J. Geotech. Geoenviron. Eng.*, **136**(8), 1148-1160. https://doi.org/10.1061/(ASCE)GT.1943-5606.0000316.

Zhao, H.H., Ge, L. and Luna, R. (2010), "Low viscosity pore fluid to manufacture transparent soil", *Geotech. Test. J.*, **33**(6), 1-6. https://doi.org/10.1520/GTJ20160163.

Zhang, L. and Zhao, M.H. (2015), "Deformation analysis of geotextile-encased stone columns", *Int. J. Geomech.*, **15**(3), 04014053. https://doi.org/10.1061/(ASCE)GM.1943-5622.0000389.

CC

Appendix: Theoretical predicted

In the theoretical model (Kong *et al*. 2018), it was assumed that the geotextile material behaves as an elastic material with a constant stiffness modulus and the stone column rests on a hard stratum. The confining stress acting on the column is derived via two approaches: the lateral confining stress provided by the surrounding soil and the additional confining stress provided by geotextile. The deformation (δ_c and S_c) of the stone column can be derived as

$$\delta_c = \frac{-B \pm \sqrt{B^2 - 4AC}}{2A} \tag{4}$$

$$S_c = \int [\frac{2\delta_c}{r_c + 2\delta_c}] dz_c \tag{5}$$

where σ_{zc} is the vertical stress of stone column, can be calculated by loading transfer $\sigma_{zc}=q_c-\int 2\tau_{cs}/r_c dz$; τ_{cs} is shear stress between column and soil, $\tau_{cs}=(p_{s0}+k_h\delta_c)\tan\varphi_{cs}$; $(p_{s0}+k_h\delta_c)$ is the earth pressure; k_h is the horizontal modulus of soil reaction, determined by $(p_{su}-p_{s0})/\triangle r_{su}$; p_{su} and p_{s0} are passive earth pressure and earth pressure at rest respectively; $\triangle r_{su}$ is the relative displacement when passive earth pressure achieves the maximum and can be taken as 0.05 m; Poisson's ratio v_c can be taken as 0.25. R_f is the parameter of stone materials, taken as 0.7. The radial bulging (δ_c) and settlement (S_c) can be obtained from equations (4) and (5), respectively. Hence, the radial bulging along the depth can be calculated through this method for comparison with the data in this paper. The parameters, A, B and C are

$$\begin{cases} A = \dfrac{2\sin\varphi_c + R_f\left(1\text{-}\sin\varphi_c\right)}{r_c}\left(\dfrac{J}{r_c^2} + k_h\right) \\ \qquad + \dfrac{\sin\varphi_c}{E_c}\left(\dfrac{J}{r_c^2} + k_h\right)^2 \\ B = \dfrac{2}{r_c}\left(P_{s0}\sin\varphi_c\right) - \dfrac{R_f\left(1-\sin\varphi_c\right)}{r_c}\left(\sigma_{zc} - P_{s0}\right) \\ \qquad + \dfrac{1}{E_c}\left(+\sin\varphi_c\left(2P_{s0} - \sigma_{zc}\right)\right)\left(\dfrac{J}{r_c^2} + k_h\right) \\ C = -\dfrac{1}{E_c}\left(\sigma_{zc} - P_{s0}\right)P_{s0}\sin\varphi_c \end{cases} \tag{6}$$